

# **Mutations within the cGMP-binding domain of CNGA1 causing autosomal recessive retinitis pigmentosa in human and animal model**

Surabhi Kandaswamy<sup>1,2,3</sup>, Lena Zobel<sup>4</sup>, Bina John<sup>5</sup>, Sathiyaveedu Thyagarajan Santhiya<sup>1</sup>, Jacqueline Bogedain<sup>4,6</sup>, Gerhard K.H. Przemeck<sup>7,8</sup>, Valérie Gailus-Durner<sup>7</sup>, Helmut Fuchs<sup>7</sup>, Martin Biel<sup>6</sup>, Martin Hrabě de Angelis<sup>7,8,9</sup>, Jochen Graw<sup>2\*</sup>, Stylianos Michalakis<sup>4</sup>, Oana Veronica Amarie<sup>7</sup>

<sup>1</sup>Dr. ALM PG IBMS, University of Madras, Taramani Campus, Chennai – 600 113, India.

<sup>2</sup>Institute of Developmental Genetics, Helmholtz Zentrum München, German Research Center for Environmental Health, Neuherberg, Germany.

<sup>3</sup>present address: Manchester Centre for Genomic Medicine, School of Biological Sciences, The University of Manchester, St Mary's Hospital, Oxford Road, Manchester M13 9WL.

<sup>4</sup>Department of Ophthalmology, University Hospital, Ludwig-Maximilians-Universität München, Munich, Germany.

<sup>5</sup>Rajan Eye Care Hospital, T Nagar, Chennai, India.

<sup>6</sup>Department of Pharmacy – Center for Drug Research, Ludwig-Maximilians-Universität München, Munich, Germany.

<sup>7</sup>Institute of Experimental Genetics and German Mouse Clinic, Helmholtz Zentrum München, German Research Center for Environmental Health, Neuherberg, Germany.

<sup>8</sup>German Center for Diabetes Research (DZD), Ingolstädter Landstr. 1, 85764 Neuherberg, Germany.

<sup>9</sup>Chair of Experimental Genetics, TUM School of Life Sciences, Technische Universität München, Alte Akademie 8, 85354 Freising, Germany.

27 \* Retired, ORCID-ID: 0000-0003-0298-9660

28

## 29 Corresponding Authors

30 Oana Veronica Amarie (ORCID-ID: 0000-0003-1705-6812), +49-89 3187-

31 4478; [oana-veronica.amarie@helmholtz-muenchen.de](mailto:oana-veronica.amarie@helmholtz-muenchen.de) ; Surabhi

32 Kandaswamy (ORCID-ID: 0000-0002-6336-1722);

33 [surabhi.kandaswamy@gmail.com](mailto:surabhi.kandaswamy@gmail.com) ; Stylianos Michalakis (ORCID-ID: 0000-

34 0001-5092-9238); [stylianos.michalakis@med.lmu.de](mailto:stylianos.michalakis@med.lmu.de)

35

## 36 ABSTRACT

37 Retinitis pigmentosa is a group of progressive inherited retinal dystrophies  
38 that may present clinically as part of a syndromic entity or as an isolated  
39 (nonsyndromic) manifestation. In a family suffering from retinitis  
40 pigmentosa, we identified a missense variation in *CNGA1* affecting the  
41 cyclic nucleotide binding domain (CNBD) and characterized a mouse model  
42 developed with mutated CNBD. A gene panel analysis comprising 105  
43 known RP genes was used to analyze a family with autosomal-recessive  
44 retinitis pigmentosa (arRP) and revealed that *CNGA1* was affected. From  
45 sperm samples of ENU mutagenesis derived F<sub>1</sub> mice, we re-derived a  
46 mutant with a *Cnga1* mutation. Homozygous mutant mice, developing  
47 retinal degeneration, were examined for morphological and functional  
48 consequences of the mutation. In the family, we identified a rare *CNGA1*  
49 variant (NM\_001379270.1) c.1525G>A; (p.Gly509Arg), which co-  
50 segregated among the affected family members. Homozygous *Cnga1* mice  
51 harboring a (ENSMUST00000087213.12) c.1526A>G (p.Tyr509Cys)  
52 mutation showed progressive degeneration in the retinal photoreceptors  
53 from 8 weeks on. This study supports a role for *CNGA1* as a disease gene  
54 for arRP and provides new insights on the pathobiology of cGMP-binding  
55 domain mutations in *CNGA1*-RP.

56 **Keywords:** *CNGA1*, retinitis pigmentosa, autosomal recessive, rod-  
57 degeneration, mouse model

---

58

## 59 INTRODUCTION

60 Retinitis pigmentosa (RP) is a group of Inherited Retinal  
61 Degeneration/Dystrophies (IRD), with a global prevalence of 1 in 3000 –  
62 7000 (1). RP is characterized by abnormalities in the photoreceptors (rods  
63 and cones) or the retinal pigment epithelium (RPE) with all types of  
64 inheritance patterns documented. RP can occur either as isolated or as  
65 syndrome with the involvement of other organs such as the associated  
66 hearing loss in USHER syndrome. About 90 genes are known until date to  
67 cause RP (Retnet database <http://www.sph.uth.tmc.edu/retnet/>). Most of the  
68 gene variants in RP are directly associated with the phototransduction  
69 cascade, such as *RHO* (rhodopsin), which are known to cause 25-30% of  
70 adRP. Phototransduction begins with the detection of light photons by  
71 rhodopsin, and this triggers several signaling steps that eventually convert  
72 the light signal into an electrical signal being transmitted to the brain. Key  
73 steps of this downstream signaling are mediated by proteins encoded by  
74 genes linked to RP. This list includes genes encoding for the subunits of rod  
75 phosphodiesterase (*PDE6A* and *PDE6B*) and rod cyclic nucleotide gated  
76 (CNG) channel (*CNGA1* and *CNGB1*). *CNGA1* encodes the A (or alpha)  
77 subunit of the rod CNG channel, which is a heterotetrameric channel  
78 complex formed by three *CNGA1* and one *CNGB1* subunits; its structure  
79 has been recently solved (2). The rod CNG channel along with *CNGB1*  
80 forms a cyclic guanosine monophosphate (cGMP)-gated cation channel  
81 found in the rod photoreceptor outer segment plasma membrane (3). Each  
82 CNG channel subunit consist of six transmembrane domains, and both, the  
83 N-terminal and the C-terminal domain, are in the cytoplasm (2). While the  
84 A subunit is essential for the principle formation of a functional cGMP-

gated channel, the B subunit is important for transport of the channel to the plasma membrane of the rod outer segment and confers specific properties to the channel complex such as rapid on-off kinetics and sensitivity to the pharmacological inhibitor L-cis-diltiazem (4,5).

In the present study we report a rare variant (c.1525G>A; p.Gly509Arg) of the *CNGA1* gene in a family suffering from arRP. Animal models for retinal degeneration usually provide insights into pathological mechanism of disease progression and assist in designing therapeutic strategies. We re-derived a *Cnga1* (c1526A>G; pTyr509Cys) mouse mutant from the ENU archive (6). This mutation falls within the same protein domain as the one observed in the human family. We report herein the retinal degeneration by a longitudinal morphological and physiological analysis.

97

## 98 MATERIALS AND METHODS

### 99 Clinical diagnosis and case recruitment

A male in his early 20s was registered with a complaint of night blindness at the retinal unit of the Eye Care Hospital. Detailed case history was recorded through a questionnaire designed for the study. Pedigree history revealed multiple affected family members including proband's grandparent and two relatives. The study protocol was in accordance with the ethical guidelines of the 1975 Declaration of Helsinki. Written informed consent regarding publishing of their data and photographs, was obtained from all participants and study subjects were anonymized by specific internal codes. The study involving human subjects was approved by the Madras Medical College Institutional Ethical committee review board and all participants have signed a written informed consent when recruited (Approval no - 29022013).

### 112 Molecular analysis

113 To dissect the molecular pathology of the affected family, targeted retinal  
114 panel sequencing (TRPS) covering 105 genes involved in retinal dystrophies  
115 was performed at Medgenomics (Kochi, India); it included DNA library  
116 preparation, enrichment capture of exonic regions of the selected 105 genes  
117 (Supplementary table 1), cluster amplification, sample run on the Illumina  
118 HiSeq platform, and generation of raw data for further analysis. The data  
119 generated by TRPS were annotated and filtered based on the positive indels  
120 (above 35%), zygosity (homozygous/heterozygous), and analysis in the  
121 context of the disease (clinical documentation and phenotype) applying  
122 ACMG Criteria (7). The putative disease-causing variant was crosschecked  
123 among affected family members, among available unaffected family  
124 members and 120 unrelated control subjects of same ethnicity using custom-  
125 designed primers (Supplementary table 2) by direct sequencing.

#### 126 **Structural comparison of CNGA1 wild-type protein versus mutant** 127 **proteins (Human – CNGA1<sup>Gly509Arg</sup>; Mouse- CNGA1<sup>Tyr509Cys</sup>)**

128 Structural models of CNGA1 proteins were generated using the  
129 RoseTTAfold deep learning algorithm (8) available at  
130 <https://robetta.bakerlab.org/>. The protein data bank (PDB) file 7RHH (9)  
131 was used as template structure. Sequences of human CNGA1 wild-type and  
132 respective mutant were obtained and based on protein isoform 2  
133 (NP\_000078.3). Sequences of mouse CNGA1 wild-type and respective  
134 mutant were based on NP\_031749.2. Sequences were obtained from NCBI.  
135 Since the published sequence/structure is shorter than the known protein  
136 sequences, the wild-type and mutant sequences of both human and mouse  
137 CNGA1 were truncated accordingly. The generated 3D models were  
138 visualized using the UCSF Chimera software  
139 (<https://www.cgl.ucsf.edu/chimera/>).

#### 141 **Generation of *Cnga1*<sup>Y509C</sup> homozygous mice**

142 ENU mutagenesis was performed as described previously (10). Briefly, ten-  
 143 week-old C3HeB/FeJ male mice were injected intraperitoneal with ENU  
 144 (three doses of 90 mg/kg in weekly intervals). First generation (F1) founder  
 145 male mice were cryo-archived by their sperm and spleen-derived DNA  
 146 samples. The DNA archive was screened for variants in the *Cnga1* gene  
 147 affecting the cytoplasmic domain. The respective sperm sample was used to  
 148 generate mice by *in vitro* fertilization and embryo transfer. The mutation  
 149 was confirmed through PCR-based direct sequencing with custom-designed  
 150 primers *Cnga1Ex9LI*: 5'-TGAGAGAGAAGTCCTGAGATACC-3' and  
 151 *Cnga1Ex9RI*: 5'-TGAGGTCATCTTTGGAGAGGC-3' (Supplementary  
 152 table 2). We established the *Cnga1* mutant line by repeated outcrossing with  
 153 C57BL/6J mice to eliminate unwanted ENU mutations and the *Pde6b*  
 154 mutation present in the C3HeB/FeJ genetic background (11). Mice were  
 155 kept in pathogen-free quarters under a 12 h light/dark cycle and had *ad*  
 156 *libitum* access to chow diet and water. All animal experiments were  
 157 conducted in accordance with the German Law of Animal Protection and  
 158 were approved by the government of upper Bavaria (Approval no - 55.2-1-  
 159 54-2532-80-16).

## 160 **Spectral-domain optical coherence tomography**

161 Optical coherence tomography was performed with an SD-OCT system  
 162 (Spectralis®, HRA+OCT Heidelberg Engineering, Heidelberg, Germany) as  
 163 described by Pawliczek et al. (12) and Schön et al. (13). Retinal sagittal  
 164 sections were obtained along horizontal meridian, centered on the optic  
 165 nerve. In addition, fundus BluePeak autofluorescence (BAF) and OCT  
 166 angiography images (OCTA) were recorded. Mice were anaesthetized with  
 167 ketamine (100 mg/kg)/xylazine (10 mg/kg) for the *in vivo* imaging and for  
 168 the retinal function test. Mice were sacrificed by carbon dioxide.

## 169 **Electroretinography**

Longitudinal ERG was performed in anesthetized animals (n = 8–14 per age group) after overnight dark adaptation using Celeris (Diagnosys LLC, Littleton, USA), as previously described by Wagner et al. (14). Briefly, pupils were dilated, and light guide electrodes were placed on both eyes centrally. Dark-adapted single flash intensity and flicker frequency series data were recorded. Stimuli of different light intensities were applied to the eyes, and the responses were recorded by the ERG device. Seven different stimuli ranging from 0.01 to 10 cd s m<sup>-2</sup> were used for single flash measurements, which were based on the International Society for Clinical Electrophysiology of Vision (ISCEV) standardized protocol for clinical dark-adapted ERG recordings (15).

# **Western blot**

Protein lysates were obtained from retinas of 1 month old (PM1) and 6 months old (PM6) wild-type and *Cngal*<sup>Y509C/Y509C</sup> mice by disrupting the tissue with a mixer mill and extracting the proteins in RIPA lysis buffer (Merck, Darmstadt, Germany). Equal amounts of proteins were separated using 6-12 % SDS-PAGE, followed by Western blot analysis according to standard procedures. The following antibodies were used: rabbit anti-CNGA1 (1μg/mL), custom-made against the 19-mer Cys-RLTKVEKFLKPLIDTEFS-HN2, corresponding to 727–744 of human CNGA1 (NP\_001136036.1); rabbit anti-CNGB1 1μg/mL, #4678 (16), anti-β-actin-peroxidase 1:25000 (A3854, Sigma-Aldrich, Saint Louis, USA), mouse anti-rabbit IgG-HRP 1:2000 (Sc-2357, Santa Cruz Biotechnologies, USA). Quantification was done using Image Lab Software Version 5.0 (Bio-Rad Laboratories, Munich, Germany).

# **Histopathology**

Eyes obtained from PM1, PM2 and PM4 controls and mutant mice were fixed 24 hrs in Davidson solution, dehydrated in 100% ethanol for 3 times (each for 15 min), embedded in Technovit® 8100 (Heraeus Kulzer,

Wehrheim, Germany) and kept for polymerization for 6-10 hours at 4°C. Sagittal 2 µm sections through the middle of the eye ball were stained with basic fuchsin and methylene blue (BF&Me). Slides were scanned (NanoZoomer 2.0HT digital slide scanner, Hamamatsu, Japan) and taken images were processed with Adobe Illustrator image-processing program (17).

## Immunohistochemistry

Immunohistochemical staining was performed on sagittal cryo-sections of PM1, PM3, PM6, PM9 and PM12 retinas (13,16). We used the following primary antibodies: rabbit anti-CNGA1 (1:3000), custom-made against the peptide Cys-RLTKVEKFLKPLIDTEFS-HN2, corresponding to 727–744 of human CNGA1 (NP\_001136036.1), rabbit anti-CNGB1 1:5000, #4678 (16), custom-made against the lectin anti-PNA FITC-conjugated 1:500 (#L7381, Sigma-Aldrich, Saint Louis, USA) and DAPI 1µg/mL. Laser scanning confocal micrographs were collected using a Leica SP8 confocal system (Leica, Wetzlar, Germany) equipped with the following lasers: 405, 448, 514, and 552 nm. Images were acquired as confocal z stacks using LAS X software V3.5.1.18803 (Leica). Maximum projection (merging of all z stacks) and background subtraction (value of 30) was performed using Fiji ImageJ V2.1.0/1.53c software (18).

## Real-Time quantitative Reverse Transcription PCR

Retinas were dissected and total RNA was isolated using the RNeasy Plus Mini Kit (Qiagen, Hilden, Germany). First-strand cDNA was synthesized from equal amounts of RNA with the RevertAid First Strand cDNA Synthesis Kit (Thermo Fisher Scientific, Waltham, USA). RT-qPCR was performed using the QuantStudio™ 5 Real-Time PCR System (Applied Biosystems, Taufkirchen, Germany). PowerUp SYBR Green Master Mix

(Applied Biosystems) was used for quantification of amplified PCR products using specific primers for *Cngal* (forward 5'-CTGTGAAGCTGGTCTGTTGG-3'; reverse 5'-TAACTGCCGTCACCTCAACAC-3'), *Cngbl* (forward 5'-TCTGAACAGGTGTCAGGATGTT-3'; reverse 5'-CTGTTTCTGGCTGTGGTCCT-3') and *mALAS* (forward 5'-TCGCCGATGCCCATCTTATC-3'; reverse 5'-GGCCCCAACTTCCATCAT CT-3').

## Statistics

Statistical analyses were performed using Prism 9 (GraphPad Software, San Diego, USA). Results are given as mean  $\pm$  SEM or SD as indicated. Measured values of  $p \leq 0.05$  were considered significant. It is defined precisely as follows: \* $p \leq 0.05$ , \*\* $p < 0.01$ , \*\*\* $p < 0.001$ .

## RESULTS

### Clinical and molecular analysis of the affected family

The male in his 20s patient had bilateral progressive loss of night vision. Family history revealed autosomal recessive inheritance (Fig. 1A, full pedigree can be requested from the corresponding author). Fundus examination of the proband revealed pigmentary deposits in the periphery and the macular region, attenuated arterioles and waxy pallor disc (Fig. 1B). OCT examination revealed thinning of all retinal layers and a medium reflective lumpy lesion from the RPE suggesting lipofuscin deposits between the RPE and the photoreceptor layer. The surrounding black area denotes the subretinal fluid collection (Fig. 1C). This family was clinically diagnosed with early onset retinitis pigmentosa.

253 A rare homozygous variant in the gene *CNGA1*, (c.1525G>A; p.Gly509Arg  
254 was documented by TRPS (Fig. 2A). In affected family members, PCR  
255 based direct sequencing was resorted because no restriction site was  
256 available. The variant co-segregate amongst affected family members of  
257 proband, and two of his relatives, while the unaffected family members  
258 (proband's parents, sibling, and the rest of the relatives were heterozygous  
259 carriers (Supplementary-Fig1)). This variant co-segregates amongst affected  
260 family members and is absent in 120 ethnically matched controls. The same  
261 variant ((NM\_000087.3) c.1537 G > A; p.Gly513Arg) was earlier reported  
262 in association with another disease-causing variant as compound  
263 heterozygous condition underlying autosomal recessive retinitis pigmentosa  
264 in a Chinese family (19). Furthermore, this is also reported in the population  
265 database at a very low frequency (gnomAD exomes -0.000008029  
266 (2/249086); (gnomAD genomes - 0.00001972 (3/152130) and no  
267 homozygotes were observed - Supplementary table 3). Both, the nucleotide  
268 (PhyloP score-5.885 and PhastCons score-1) and amino acid, are highly  
269 conserved across species (considering 14 species up to *C. elegans*) (Fig.2B).  
270 *In-silico* tools (Supplementary table 3), as well as applying ACMG criteria,  
271 predicted and classified this variant as pathogenic. To better visualize the  
272 mutated amino acid in the channel context, we performed RosettaFold-based  
273 modelling of wild-type and mutant CNGA1 proteins. Although RosettaFold  
274 only models the protein, not the cGMP molecule, it revealed that the mutant  
275 Arg509 (which is positioned at 509 in NP\_001366199.1, p.Gly509Arg)  
276 protrudes into the inner space of the cGMP binding pocket (in Fig.2 C:  
277 compare the models with the cGMP-bound cryo-electron microscopy  
278 structure). Given that Arg is a basic amino acid, and occupies more space  
279 than Gly, which is neutral and allows for less flexibility of the amino acid  
280 chain, this substitution is expected to alter the overall secondary structure of  
281 the cyclic nucleotide-binding domain (CNBD) and the cGMP binding  
282 pocket (Fig.2 C).

## 283 **Generation of *Cnga1* mutant mice**

284 From the DNA archive of ENU-induced mutant mice, we identified the  
285 missense mutation c.1526 A>G (Fig.3 A, B) in the *Cnga1* gene, leading to a  
286 substitution of Tyr509 by Cys. Mouse Tyr509 corresponds to Tyr513 in the  
287 human CNGA1 protein and thus affects a residue only 4 amino acids away  
288 from the mutant Arg509 in the human patient. Polyphen-2 predicted a  
289 probably damaging effect of this mutation (score 1.000), because this  
290 Tyr509 residue is highly conserved across a variety of species. Again, we  
291 performed RosettaFold-based modelling to visualize the wild-type and  
292 mutant CNGA1 proteins and again observed a slightly changed CNBD and  
293 cGMP binding pocket structure (Fig. 3 C).

## 294 **Rod CNG channel expression in *Cnga1* mutant mice**

295 We first analysed the effect of the mutation on the expression of the rod  
296 CNG channel homozygous *Cnga1* mutants. To determine the expression  
297 pattern of CNGA1, we immunolabeled retinal cross-sections of wild-type  
298 and *Cnga1* mutant mice for CNGA1 and CNGB1 proteins. In the wild-type  
299 retina, we observed a strong and specific immunofluorescence signal for  
300 both CNGA1 and CNGB1 in rod outer segments of one-month-old (PM1)  
301 mice (Fig. 4 A, D). In contrast, under the same imaging conditions, no  
302 CNGA1 signal was observed in the *Cnga1* mutant retina (Fig. 4 B). In six-  
303 month-old (PM6) mice, the CNGA1 immunosignal was also absent, in  
304 addition to a marked thinning of the outer nuclear layer (Fig. 4 C).  
305 Interestingly, the mutant retinas were also immunonegative for CNGB1  
306 indicating degradation of the CNGB1 protein in the absence of CNGA1  
307 (Fig. 4 E – F). Western blot analysis on retinal lysates detected the  
308 corresponding proteins in the wild type and confirmed the reduction of both  
309 CNG channel subunits in the mutant (Fig. 4 G – I, uncropped Western blots  
310 in Supplementary Figure 2). Analysis of the corresponding gene expression  
311 by qRT-PCR revealed similar levels of *Cnga1* mRNA transcript at 1 month

312 of age and significantly decreased levels at PM6, when substantial ONL loss  
313 had occurred (Fig. 4 J). The levels of *Cngbl* mRNA were already slightly  
314 downregulated at PM1 and further decreased at PM6 (Fig. 4 K). These  
315 findings suggest that the *Cnga1* mutation does not impair principle gene  
316 expression and most likely exerts its negative effect at the protein level.

### 317 **Retinal function in *Cnga1* mice**

318 Next, we assessed retinal function in *Cnga1* mutant mice by  
319 electroretinography (ERG). Mice were evaluated starting at postnatal week  
320 3 (PW3), PM1, PM3, PM6, PM9 and PM12 to track functional changes over  
321 time. Scotopic and photopic ERG protocols were applied to evaluate rod-  
322 and cone-mediated light responses. Representative scotopic ERG traces and  
323 corresponding quantifications of the ERG a- and b-wave amplitudes are  
324 shown in Fig. 5. In wild-type mice, a- and b-wave amplitudes were clearly  
325 visible and showed an expected slight age-dependent decline over time (Fig.  
326 5 B and E). In contrast, we could not detect any rod-derived a-wave in  
327 *Cnga1* mutant mice (Fig. 5 B, C and D), suggesting that mutant rods are  
328 incapable of generating light responses. The ERG b-wave was also absent  
329 after stimulation with rod-specific low luminance (0.01 or 0.03 cd.s/m<sup>2</sup>) and  
330 decreased strongly at higher luminance (Fig. 5 E, F and G). From PM9  
331 onwards, *Cnga1* mutant mice no longer respond to light stimuli, since no  
332 ERG response was detectable even at the highest luminance (10 cd.s/m<sup>2</sup>)  
333 (Fig. 5 A, E and G). In summary, ERG analysis indicates a lack of rod  
334 photoreceptor-driven responses in *Cnga1* mutant mice as early as PW3 and  
335 reveals a secondary, slowly progressive loss of cone-mediated light  
336 responses, leading to complete blindness after PM9.

### 337 **Rod degeneration in homozygous *Cnga1* mutant mice**

338 The *Cnga1* mutation affects the morphology of the mouse retina (Fig. 6 A).  
339 While the overall lamination of the retina appeared to be preserved in the  
340 morphology of *Cnga1* mutant mice at PM1, PM2 and PM4, there was early

341 shortening of the outer and inner segments of the photoreceptor layers, and  
 342 at PM4, we found a marked thinning of the outer nuclear layer (ONL) (Fig.  
 343 6 A). Rhodopsin, a marker of rod outer segments, was stained in wild-type  
 344 and *Cnga1*<sup>Y509C/Y509C</sup> mouse retinas at PM1, PM3, PM6, PM9 and PM12.  
 345 Indeed, the rhodopsin staining shows gradually reduction of rhodopsin  
 346 expression in the mutant retina over time, revealing a compromised  
 347 morphology of rod outer segments already at PM1 (Supplementary Figure  
 348 3).

349 To better characterize the progression of degeneration we performed a  
 350 longitudinal *in vivo* spectral domain optical coherence tomography (SD-  
 351 OCT) imaging study comparing *Cnga1* mutant mice to healthy age-matched  
 352 wild-type mice (Fig. 6 B - F). SD-OCT evaluation of the entire  
 353 photoreceptor length, measured as the combined thickness of the outer  
 354 segment and the ONL layer (hereafter referred to as photoreceptor plus or  
 355 PhR+), revealed an initial loss of 15 – 20 % of the PhR+ layer at PW3, PW4  
 356 and PM2 (Fig. 6 F). While the PhR+ layer thickness remained stable in the  
 357 healthy control, it steadily declined over time in the *Cnga1* mutant (Fig. 6  
 358 F). Between PM5 and PM6 half of the PhR+ layer was lost in the mutant.  
 359 Degeneration slowed after PM7, culminating in an almost complete loss of  
 360 the PhR+ layer at PM12, and only the inner nuclear (INL) and ganglion cell  
 361 (GCL) layers remained (Fig. 6 E, F). However, at PM12 the appearance of  
 362 the INL nuclei starts to be more scattered, suggesting the appearance of  
 363 secondary morphological changes in this inner retinal layer.

# **364 Secondary degeneration of non-rod cells in *Cnga1* mice**

365 *In vivo* BluePeak autofluorescence (BAF) and OCT angiography (OCT-A)  
 366 were used to examine the morphology of the retinal fundus and the retinal  
 367 vasculature (Fig. 7 A, B). At PM4, BAF imaging revealed accumulation of  
 368 autofluorescent material in the fundus of *Cnga1* mutant mice (Fig. 7 A). In  
 369 OCT-A scans, we observed altered vascular bed density in the mutant and a

370 thinner appearance of the large blood vessels (Fig. 7 B). The SD-OCT and  
371 OCT-A measurements suggested the occurrence of secondary changes in  
372 non-rod cells as rod degeneration progresses. In order to analyse the  
373 morphology of cone photoreceptors over time, we labeled retinal sagittal  
374 sections of PM1, PM3, PM6, PM9 and PM12 wild-type and *Cnga1* mutant  
375 mice with the cone-specific marker peanut agglutinin (PNA), which labels  
376 the extracellular matrix of cone photoreceptors (20) (Fig. 7 C - H). At PM1,  
377 cone morphology, as judged by the PNA signal, appeared similar in both  
378 genotypes (Fig. 7 D). Over time, a gradual reduction of PNA signal was  
379 observed, revealing a loss of the outer segments of cones at PM9 and a  
380 complete loss of the cones at PM12 (Fig. 7 E - H).

381

## 382 DISCUSSION

383 In the present study, we have identified a family with autosomal  
384 recessive retinitis pigmentosa suffering from a homozygous c.1525G>A  
385 (NM\_001379270.1) missense mutation in *CNGA1* leading to substitution of  
386 a Gly at position 509 by an Arg. So far, this mutation (previously recorded  
387 as c.1537 G > A; p.Gly513Arg (NM\_000087.3)) has only been found as  
388 heterozygous in patients with retinitis pigmentosa (19). The same study  
389 described that transfection of HEK293 cells with the c.1537 G>A mutant  
390 *CNGA1* results in similar protein expression levels as the wild-type *CNGA1*  
391 (19). Gly509 is part of the loop linking two  $\beta$ -strands ( $\beta$ 2 and  $\beta$ 3) within the  
392 CNBD. While Gly509 is not directly involved in cGMP binding, it is most  
393 likely important for the flexibility of the  $\beta$ 2/ $\beta$ 3-connecting loop and thus for  
394 CNBD structure and function. In line with an important role, this glycine is  
395 conserved between species but also within the CNG channel family (4).

396 *CNGA1* was one of the first genes linked to RP over 27 years ago  
397 (21). To date, almost 50 probable pathogenic mutations in *CNGA1* have  
398 been identified (1) and a prevalence ranging of 2 % of arRP cases in Spain

(22) to 7.6% in China (23) has been estimated. Despite its early discovery, little is known about *CNGA1*-RP, partly due to the lack of adequate animal models. More than 20 years ago a mouse model expressing an 890 bp *Cnga1* antisense DNA fragment was generated (24). A slight retinal degeneration was noted at 1 year of age (24). Since the effect of antisense expression was not confirmed at the protein level, it is unclear to what extent the observed morphological changes are due to a loss of CNGA1. Moreover, a functional characterization of this transgenic mouse line is missing. In 2015, the identification of a naturally occurring canine model with a mutation in the *Cnga1* gene was reported (25) providing a first genetic and clinical description. However, no detailed information on the retinal phenotype has been described. More recently, a mouse model with a targeted deletion in exon 2 of *Cnga1* was reported (26). This model carries an engineered 65 bp frame-shift deletion that, although not experimentally verified at the protein level, should result in a premature stop codon shortly after the deletion and loss of most of the ion channel protein. *Cnga1*-deficient mice were shown to lose the majority of photoreceptors by 16 weeks (26). Scotopic ERG responses to a single flash of 3 cd\*s/m<sup>2</sup> in these mice were greatly reduced at 3 weeks, which further decreased after 10 weeks (26).

Because the mutation identified in the here presented family results in a single amino acid exchange in the CNBD, this prompted us to develop an animal model that mimics this type of mutation. Indeed, we have identified from the ENU mutagenesis repository at the Helmholtz Center a mouse mutant with a c.1526 A>G mutation in *Cnga1*, resulting in a Tyr509Cys exchange in the CNBD of the CNGA1 protein. Tyr509 corresponds to Tyr513 in the human CNGA1 protein and participates in the formation of the  $\beta$ 3 strand of the CNBD (4). This Tyr residue is conserved in the various mammalian CNG channel subunits and is even found in hyperpolarization-activated and cyclic nucleotide-gated channels (HCN),

429 cGMP-regulated protein kinase 1 (PRKG1) or the cAMP-regulated protein  
430 kinase catalytic subunit (PRKACA). Interestingly, the structurally related  
431 potassium voltage-gated channel subfamily H member 1 (KCNH1), which  
432 contains a presumably non-functional CNBD and cannot be gated or  
433 modulated by cyclic nucleotides (27), has a Cys instead of Tyr at the  
434 corresponding position (aa 619). Although the mutation found in the ENU  
435 mouse model does not affect the same Gly residue as the c.1525 G > A  
436 mutation found in the patients, it affects a Tyr residue just four amino acids  
437 downstream from Gly509 and is thought to mimic the human Gly509Arg  
438 substitution.

439 Analysis of the CNG channel expression in 1 month old  
440 *Cnga1*<sup>Y509C/Y509C</sup> mutant mice revealed an almost complete lack of CNGA1  
441 protein, but normal *Cnga1* transcript levels. While *Cngb1* mRNA levels  
442 were also unaffected, we could not detect any CNGB1 protein in  
443 *Cnga1*<sup>Y509C/Y509C</sup> at 1 month of age. This is in line with similar observations  
444 in *Cngb1*-deficient mice (16) and dogs (28), in which the absence of the  
445 CNGB1 subunit led to degradation of the remaining CNGA1 protein,  
446 although the *Cnga1* transcript was unaffected. It appears that the Tyr509Cys  
447 mutation has a major effect on protein structure and/or stability, resulting in  
448 a complete loss of the anti-CNGA1 immunosignal in Western blot and  
449 immunohistochemistry. Consistent with the loss of rod CNG channel  
450 function, we observed an absence of rod-driven ERG responses (a- and b-  
451 wave) from the earliest observation time point (PW3). This differs from  
452 what has been described in the *Cnga1* knockout mouse (26), but is most  
453 likely due to the fact that we used rod-specific ERG stimuli (e.g., the ISCEV  
454 rod stimulus: 0.03 cd.s/m<sup>2</sup>), while Liu et al. (26) used only a 3 cd.s/m<sup>2</sup>  
455 stimulus, which elicits a mixed rod and cone response and therefore does  
456 not allow for segregation or distinct of rod-specific responses.

457 To gain a better understanding of the progression rate of rod and  
458 cone degeneration, we performed a 1-year *in vivo* imaging study with 13

459 observation time points. This allowed us to define with high granularity the  
460 time course of rod loss and the onset of secondary cone degeneration.  
461 Again, we observed differences between the *Cnga1*<sup>Y509C/Y509C</sup> mouse line  
462 with a point mutation and the homozygous *Cnga1* knockout mouse. Liu et  
463 al. (26) showed retinal thickness measurements up to 4 months, while we  
464 followed the progression of retinal degeneration over 12 months. After 4  
465 months, the thickness of the photoreceptor layer was reduced to only 20 %  
466 in the *Cnga1* knockout, but to about 60 % in the *Cnga1*<sup>Y509C/Y509C</sup> mouse.  
467 The reason for the slow degeneration in these two mouse lines is not clear.  
468 In our Western blot and IHC analyses, we observed an almost complete loss  
469 of CNGB1 and CNGA1 proteins as early as 1 month. Since protein data are  
470 missing from the Liu et al. study (26), we can only assume that the rod CNG  
471 channel proteins are also missing in the *Cnga1* knockouts. In contrast to  
472 primary rod degeneration, secondary degeneration of cone photoreceptors  
473 appears to have a similar rate of progression in both mouse models.  
474 In conclusion, single point mutations in the CNBD of the A subunit of the  
475 rod CNG channel are not tolerated and results in loss of both channel  
476 subunits at the protein level and eventual loss of function of this important  
477 ion channel of the rod photoreceptor transduction cascade. The  
478 *Cnga1*<sup>Y509C/Y509C</sup> mouse appears to be an appropriate model of *CNGA1*-arRP  
479 and should be of great value for future studies on the molecular  
480 characterization of the pathobiology involved in the disease. Finally, the  
481 *Cnga1*<sup>Y509C/Y509C</sup> mouse is a suitable model for preclinical proof-of-concept  
482 studies for future therapeutic approaches to treat this blinding disease.

### 483 **Acknowledgement**

484 The authors thank Erika Bürkle, Monika Stadler and Andreas Mayer for  
485 expert technical assistance. SK thanks the German Academic Exchange  
486 Service (DAAD) (Funding no - 91525094) for her research stay in Germany  
487 (2014-2016), UGC -SRF fellowship grant and University of Madras. This

work was supported by grants from the German Federal Ministry of Education and Research (Infrafrontier grant 01KX1012 to MHdA) and the German Center for Diabetes Research (DZD) (MHdA). The authors also thank the patient's family towards their co-operation for this study.

**Conflict of interests** - The authors declare no conflict of interests.

**Data availability statement** - All data relevant to the study are included in the article or uploaded as supplementary information. The raw data that support the findings of this study are also available from the corresponding author upon request.

Reference:

1. Hanany M, Rivolta C, Sharon D. Worldwide carrier frequency and genetic prevalence of autosomal recessive inherited retinal diseases. *Proc Natl Acad Sci.* 2020 Feb 4;117(5):2710–6.
2. Xue J, Han Y, Zeng W, Jiang Y. Structural mechanisms of assembly, permeation, gating, and pharmacology of native human rod CNG channel. *Neuron.* 2022 Jan;110(1):86-95.e5.
3. Bönigk W, Altenhofen W, Müller F, Dose A, Illing M, Molday RS, et al. Rod and cone photoreceptor cells express distinct genes for cGMP-gated channels. *Neuron.* 1993 May;10(5):865–77.
4. Kaupp UB, Seifert R. Cyclic Nucleotide-Gated Ion Channels. *Physiol Rev.* 2002 Jan 7;82(3):769–824.
5. Michalakis S, Becirovic E, Biel M. Retinal Cyclic Nucleotide-Gated Channels: From Pathophysiology to Therapy. *Int J Mol Sci.* 2018 Mar 7;19(3):749.
6. Sabrautzki S, Kaiser G, Przemeck GKH, Gerst F, Lorza-Gil E, Panse M, et al. Point mutation of Ffar1 abrogates fatty acid-dependent insulin

515 secretion, but protects against HFD-induced glucose intolerance. Mol  
516 Metab. 2017 Oct;6(10):1304–12.

517 7. Richards S, Aziz N, Bale S, Bick D, Das S, Gastier-Foster J, et al.  
518 Standards and guidelines for the interpretation of sequence variants: a  
519 joint consensus recommendation of the American College of Medical  
520 Genetics and Genomics and the Association for Molecular Pathology.  
521 Genet Med. 2015 May;17(5):405–24.

522 8. Baek M, DiMaio F, Anishchenko I, Dauparas J, Ovchinnikov S, Lee  
523 GR, et al. Accurate prediction of protein structures and interactions  
524 using a three-track neural network. Science. 2021 Aug  
525 20;373(6557):871–6.

526 9. Xue J, Han Y, Zeng W, Wang Y, Jiang Y. Structural mechanisms of  
527 gating and selectivity of human rod CNGA1 channel. Neuron. 2021  
528 Apr;109(8):1302-1313.e4.

529 10. de Angelis MH, Flaswinkel H, Fuchs H, Rathkolb B, Soewarto D,  
530 Marschall S, et al. Genome-wide, large-scale production of mutant  
531 mice by ENU mutagenesis. Nat Genet. 2000 Aug;25(4):444–7.

532 11. Hart AW, McKie L, Morgan JE, Gautier P, West K, Jackson IJ, et al.  
533 Genotype–Phenotype Correlation of Mouse *Pde6b* Mutations. Investig  
534 Ophthalmology Vis Sci. 2005 Sep 1;46(9):3443.

535 12. Pawliczek D, Dalke C, Fuchs H, Gailus-Durner V, Hrabě de Angelis  
536 M, Graw J, et al. Spectral domain - Optical coherence tomography  
537 (SD-OCT) as a monitoring tool for alterations in mouse lenses. Exp  
538 Eye Res. 2020 Jan;190:107871.

539 13. Schön C, Asteriti S, Koch S, Sothilingam V, Garrido MG, Tanimoto N,  
540 et al. Loss of HCN1 enhances disease progression in mouse models of

541 CNG channel-linked retinitis pigmentosa and achromatopsia. Hum Mol  
542 Genet. 2016 Mar 15;25(6):1165–75.

543 14. Wagner JE, Zobel L, Gerhardt MJ, O’Riordan CR, Frederick A,  
544 Petersen-Jones SM, et al. *In Vivo* Potency Testing of Subretinal  
545 rAAV5.hCNGB1 Gene Therapy in the *Cngb1* Knockout Mouse Model  
546 of Retinitis Pigmentosa. Hum Gene Ther. 2021 Oct 1;32(19–20):1158–  
547 70.

548 15. Marmor MF. At Last: A Standard Electroretinography Protocol. Arch  
549 Ophthalmol. 1989 Jun 1;107(6):813.

550 16. Hüttl S. Impaired Channel Targeting and Retinal Degeneration in Mice  
551 Lacking the Cyclic Nucleotide-Gated Channel Subunit CNGB1. J  
552 Neurosci. 2005 Jan 5;25(1):130–8.

553 17. 17. Adobe Illustrator (2019) Adobe Inc., Munich, Germany.

554 18. Schindelin J, Arganda-Carreras I, Frise E, Kaynig V, Longair M,  
555 Pietzsch T, et al. Fiji: an open-source platform for biological-image  
556 analysis. Nat Methods. 2012 Jul;9(7):676–82.

557 19. Jin X, Qu L-H, Hou B-K, Xu H-W, Meng X-H, Pang C-P, et al. Novel  
558 compound heterozygous mutation in the *CNGA1* gene underlie  
559 autosomal recessive retinitis pigmentosa in a Chinese family. Biosci  
560 Rep. 2016 Feb 1;36(1):e00289.

561 20. Johnson LV, Hageman GS, Blanks JC. Interphotoreceptor matrix  
562 domains ensheath vertebrate cone photoreceptor cells. Invest  
563 Ophthalmol Vis Sci. 1986 Feb;27(2):129–35.

564 21. Dryja TP, Finn JT, Peng YW, McGee TL, Berson EL, Yau KW.  
565 Mutations in the gene encoding the alpha subunit of the rod cGMP-

- 566 gated channel in autosomal recessive retinitis pigmentosa. Proc Natl  
567 Acad Sci U S A. 1995 Oct 24;92(22):10177–81.
- 568 22. Paloma E. Novel homozygous mutation in the alpha subunit of the rod  
569 cGMP gated channel (CNGA1) in two Spanish sibs affected with  
570 autosomal recessive retinitis pigmentosa. J Med Genet. 2002 Oct  
571 1;39(10):66e–6.
- 572 23. Chen X, Zhao K, Sheng X, Li Y, Gao X, Zhang X, et al. Targeted  
573 Sequencing of 179 Genes Associated with Hereditary Retinal  
574 Dystrophies and 10 Candidate Genes Identifies Novel and Known  
575 Mutations in Patients with Various Retinal Diseases. Investig  
576 Ophthalmology Vis Sci. 2013 Mar 27;54(3):2186.
- 577 24. Leconte L, Barnstable CJ. Impairment of rod cGMP-gated channel  
578 alpha-subunit expression leads to photoreceptor and bipolar cell  
579 degeneration. Invest Ophthalmol Vis Sci. 2000 Mar;41(3):917–26.
- 580 25. Wiik AC, Ropstad EO, Ekesten B, Karlstam L, Wade CM, Lingaas F.  
581 Progressive retinal atrophy in Shetland sheepdog is associated with a  
582 mutation in the *CNGA1* gene. Anim Genet. 2015 Oct;46(5):515–21.
- 583 26. Liu Y, Wang Y, Xiao Y, Li X, Ruan S, Luo X, et al. Retinal  
584 degeneration in mice lacking the cyclic nucleotide-gated channel  
585 subunit *CNGA1*. FASEB J [Internet]. 2021 Sep [cited 2022 Apr  
586 11];35(9). Available from:  
587 <https://onlinelibrary.wiley.com/doi/10.1096/fj.202101004R>
- 588 27. Brelidze TI, Carlson AE, Zagotta WN. Absence of Direct Cyclic  
589 Nucleotide Modulation of mEAG1 and hERG1 Channels Revealed  
590 with Fluorescence and Electrophysiological Methods. J Biol Chem.  
591 2009 Oct;284(41):27989–97.

592 28. Petersen-Jones SM, Occelli LM, Winkler PA, Lee W, Sparrow JR,  
593 Tsukikawa M, et al. Patients and animal models of CNG $\beta$ 1-deficient  
594 retinitis pigmentosa support gene augmentation approach. J Clin Invest.  
595 2017 Nov 20;128(1):190–206.

596

597 Figure legends:

598 **Fig.1. Pedigree and retinal imaging of the affected family: A.**  
599 Partial five generation pedigree denoting the presence of ocular  
600 disease. Males and females, are represented by squares and circles,  
601 respectively. The symbols of affected family members are filled. **B.**  
602 Fundus images of the proband's left (L) and right (R) eye taken at  
603 the time of case registration, on one year follow-up and again at  
604 three years follow-up. Waxy pallor disc (marked by white arrow  
605 head), pigmentary deposits (marked by one sided arrow) and  
606 attenuated arterioles (marked by double sided arrow). **C.** SD-OCT  
607 images of the proband's retinal layers: left (L) and right eye (R)  
608 were taken on one year follow-up (left two panels) and three years  
609 follow-up (right two panels). Mild central hyper reflectivity  
610 suspicious of scars were marked with arrows. Thinning of the  
611 retinal layers was observed.

612

613 **Fig.2. Identification of *CNGA1* mutation: A.** Sequence  
614 chromatogram of the proband (top) and control subject from the  
615 regional population (middle) and *CNGA1* exon 10 (bottom),  
616 depicting the homozygous mutation (c.1525G>A; p.Gly509Arg);  
617 the mutant and wild-type peaks "A" and "G" are marked by  
618 arrows. The missense mutation (marked in red) is compared with  
619 the wild-type sequence (marked in green) together with the  
620 translated protein sequences. **B.** Amino acid sequence alignment of

human CNGA1 and orthologues from other species, depicting a high conservation of p.G509 (encircled in red). Divergent amino acid residues are shaded in white color background. **C.** Structural comparison of wild-type and mutant human CNGA1 (backbone is shown in grey). The amino acid of interest in the wild-type structure (Gly513, magenta) and mutant structure (Arg513, cyan) (which is position at 509 in the MANE transcript encoded protein (NP\_001366199.1) are shown as atoms. As reference structure the CNGA1 subunit of the human PDB 7RHH (9) is shown with bound cGMP (orange, shown as atom) and the residues R561, T562, A563, F544, E546, I547, S548 (grey, shown as atoms) are responsible for cGMP binding. Models were generated using the RoseTTAfold deep learning algorithm (8) available at <https://robetta.bakerlab.org/>. The generated 3D models were visualized using the UCSF Chimera software (<https://www.cgl.ucsf.edu/chimera/>).

**Fig.3. *Cnga1* mouse model:** **A.** DNA sequencing shows the mutation in the new mouse model (c. 1526□A>G; blue circles). The missense mutation (marked in red) is compared with the wild-type sequence (marked in green) together with the translated protein sequences of the mouse. **B.** Location of the human (p.Gly509Arg, top) and murine (p.Tyr509Cys, bottom) mutations in the cGMP-binding domain. **C.** Structural comparison of wild-type and mutant murine CNGA1 (backbone is shown in grey). The amino acid of interest in the wild-type structure (Tyr509, magenta) and mutant structure (Cys509, cyan) are shown as atoms. As reference structure, the CNGA1 subunit of the human PDB 7RHH [9] is shown with bound cGMP (orange, shown as atom) and the corresponding amino acid residue Tyr510 is highlighted (green).

651 Models were generated using the RoseTTAfold deep learning  
652 algorithm (8) available at <https://robetta.bakerlab.org/>. The  
653 generated 3D models were visualized using the UCSF Chimera  
654 software (<https://www.cgl.ucsf.edu/chimera/>).

656 **Fig.4. *Cnga1*<sup>Y509C/Y509C</sup> mice are lacking CNGA1 protein. (A-F)**

657 Representative confocal images showing expression of CNGA1  
658 (red) and CNGB1 protein (green) in retinal cross sections of wild-  
659 type (1 month postnatal (PM1); A, D), and *Cnga1*<sup>Y509C/Y509C</sup> mouse  
660 retinas (B-C, E-F) at PM1 and PM6. *Cnga1*<sup>Y509C/Y509C</sup> mice are  
661 lacking CNGA1 and CNGB1 already at PM1. Cell nuclei were  
662 stained with DAPI (blue). OS, outer segments; IS, inner segments;  
663 ONL, outer nuclear layer; OPL, outer plexiform layer; INL, inner  
664 nuclear layer. Scale bar marks 20  $\mu$ m. (G-I) Western blot analysis  
665 of *Cnga1*<sup>Y509C/Y509C</sup> mouse retinas at PM1 and PM6 using CNGA1-  
666 and CNGB1-antibodies.  $\beta$ -Actin was used as control. Western blot  
667 staining (G) and quantification of CNGA1 (H) and CNGB1 (I)  
668 expression confirm the findings of immunohistochemistry. (J-K)  
669 RT-qPCR of *Cnga1*<sup>Y509C/Y509C</sup> mouse retinas at PM1 and PM6 with  
670 *Cnga1*- (J) and *Cngb1*-specific primers (K). Mutant mice at PM1  
671 still express *Cnga1* and *Cngb1* transcript. This expression is  
672 reduced at PM6. N = 3 biological and technical replicates. Values  
673 are given as mean  $\pm$  SEM (one-way ANOVA paired with Tukey's  
674 post-hoc test; \*\*p $\leq$ 0.01, \*\*\*p $\leq$ 0.001).

676 **Fig.5. *Cnga1*<sup>Y509C/Y509C</sup> mice show loss of rod-driven**  
677 **electroretinography. (A)** Overlays of averaged ERG signals of  
678 *Cnga1*<sup>Y509C/Y509C</sup> mice (red) compared to wild-type mice (black) at  
679 postnatal week 3 (PW3), postnatal month 1 (PM1), PM3, PM6,

PM9 and PM12 at different light intensities. Vertical dotted lines mark the time points of light stimulation. Homozygous mutant mice show almost no (rod-mediated) response at low light intensities (0.01 and 0.03 cd s m<sup>-2</sup>) and also lose cone-mediated response between PM6 and PM9. **(B-G)** Quantification of a-wave and b-wave amplitudes of *Cnga1*<sup>Y509C/Y509C</sup> mice (red) compared to wild-type mice (black) at different ages. a-wave (B) and b-wave (E) amplitudes were massively reduced in *Cnga1*<sup>Y509C/Y509C</sup> mice compared to wild types for all light intensities at PM1. Rod-mediated responses for the a-wave (C) and b-wave (F) at a low light intensity (0.03 cd s m<sup>-2</sup>) as well as cone-mediated response for a-wave (F) at a high light intensity (10 cd s m<sup>-2</sup>) were reduced from the first measurement at PW3, while cone-mediated response for the b-wave (G) decreased over time. Wild-type mice: n=10; *Cnga1*<sup>Y509C/Y509C</sup> mice: n = 12. Values are given as mean ± SEM.

695

**Fig.6. *Cnga1*<sup>Y509C/Y509C</sup> mice show a reduced photoreceptor layer thickness.** (A) Representative retina morphology images of wild-type mice and mutants showing progressive thinning of the ONL layer in the *Cnga1*<sup>Y509C/Y509C</sup> mice. **(B-E)** Representative SD-OCT images of *Cnga1*<sup>Y509C/Y509C</sup> and wild-type mice up to 12 months of age demonstrating a massive reduction of photoreceptor layer thickness in homozygous mutant mice (C, E) compared to wild-type mice (B, D). Black bars in close-ups D and E mark the thickness of the photoreceptor layer. RPE, retinal pigment epithelium; OS, outer segments; ONL, outer nuclear layer; INL, inner nuclear layer; GCL, ganglion cell layer. **(F)** Degeneration progress of photoreceptor layer thickness in homozygous mutant mice (red) compared to wild-type mice (black) from 3 weeks until

709 12 months of age. Wild-type mice: n=10; *Cnga1*<sup>Y509C/Y509C</sup> mice: n  
710 = 12. Values are given as mean ± SD. Scale bar in A marks 100  
711 µm.

712

713 **Fig.7. *Cnga1*<sup>Y509C/Y509C</sup> mice show secondary retinal**  
714 **morphological changes and degeneration of cone**  
715 **photoreceptors. (A-B)** Representative BAF and OCT-A scans of  
716 the fundus (A) and retinal vasculature (B) showing accumulation of  
717 autofluorescent spots and altered vascular bed in the  
718 *Cnga1*<sup>Y509C/Y509C</sup> mouse fundus. **(C-H)** Representative confocal  
719 images showing expression of peanut agglutinin (PNA; green) in  
720 retinal cross sections of wild-type (1 month postnatal (PM1); (C)  
721 and *Cnga1*<sup>Y509C/Y509C</sup> mouse retinas (D-H) at PM1, PM3, PM6, PM9  
722 and PM12 demonstrating a degeneration of cone photoreceptors  
723 with age. Scale bars in B marks 200 µm. Scale bar in H marks 25  
724 µm.

725

726 **Sup-Fig.1. Sequence chromatogram of affected family**  
727 **members: *CNGA1* exon 10, depicting the homozygous mutation**  
728 **(c.1525G>A; p.Gly509Arg) in the affected family members (A, E,**  
729 **F), whereas all other unaffected family members (B, C, D, G, H)**  
730 **were heterozygous for this variant. The sequence of a control**  
731 **subject is given in I. The sites of the mutation are marked by**  
732 **arrows.**

733

734 **Sup-Fig.2. *Cnga1*<sup>Y509C/Y509C</sup> mice are lacking CNGA1 protein:**  
735 **Western blot staining of *Cnga1*<sup>Y509C/Y509C</sup> mouse retina at PM1 and**  
736 **PM6 using CNGA1- and CNGB1-antibodies. B-Actin was used as**  
737 **control. N = 3 biological and technical replicates.**

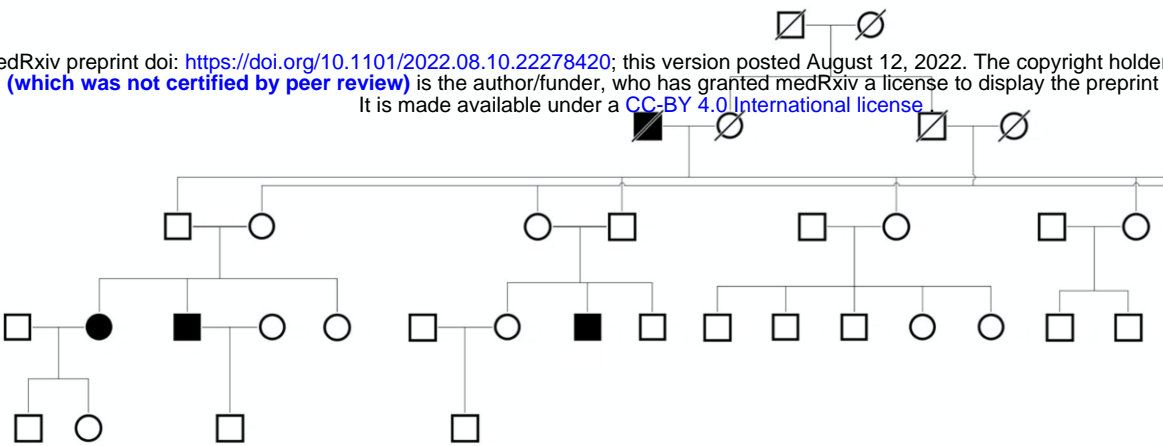
738

739 **Sup-Fig.3. *Cnga1*<sup>Y509C/Y509C</sup> mice show compromised outer**  
740 **segments morphology.** (A-F) Representative confocal images  
741 showing expression of rhodopsin (green) in retinal cross sections of  
742 wild-type at PM1 (A), and *Cnga1*<sup>Y509C/Y509C</sup> mouse retinas (B-F) at  
743 PM1, PM3, PM6, PM9 and PM12, illustrating the outer segment  
744 morphology. Rhodopsin staining shows a gradual reduction of  
745 rhodopsin expression in the mutant retina, revealing the  
746 compromised morphology of rod outer segments in the  
747 *Cnga1*<sup>Y509C/Y509C</sup> retina already at PM1. Cell nuclei were stained  
748 with DAPI (blue). OS, outer segments; IS, inner segments; ONL,  
749 outer nuclear layer; OPL, outer plexiform layer; INL, inner nuclear  
750 layer.

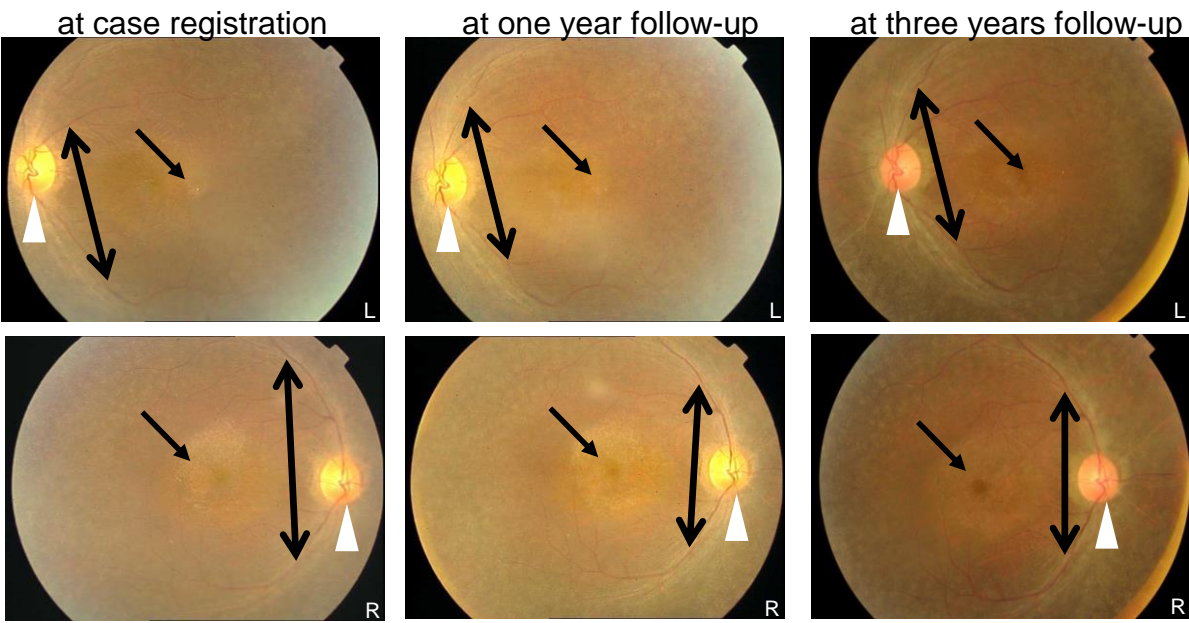
Fig. 1

A

medRxiv preprint doi: <https://doi.org/10.1101/2022.08.10.22278420>; this version posted August 12, 2022. The copyright holder for this preprint (which was not certified by peer review) is the author/funder, who has granted medRxiv a license to display the preprint in perpetuity. It is made available under a CC-BY 4.0 International license.



B



C

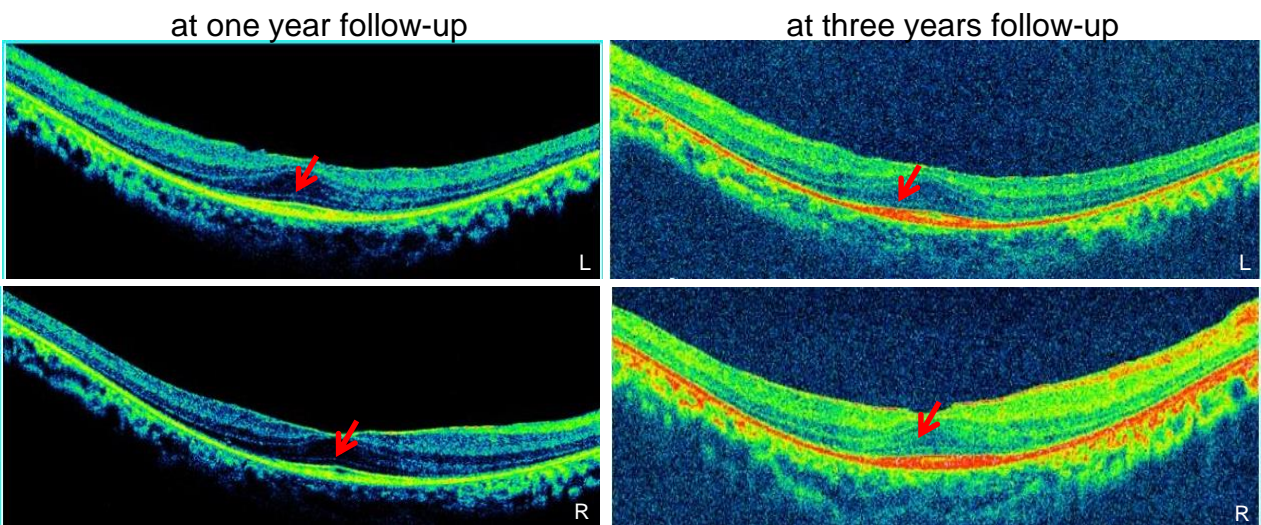


Fig.2

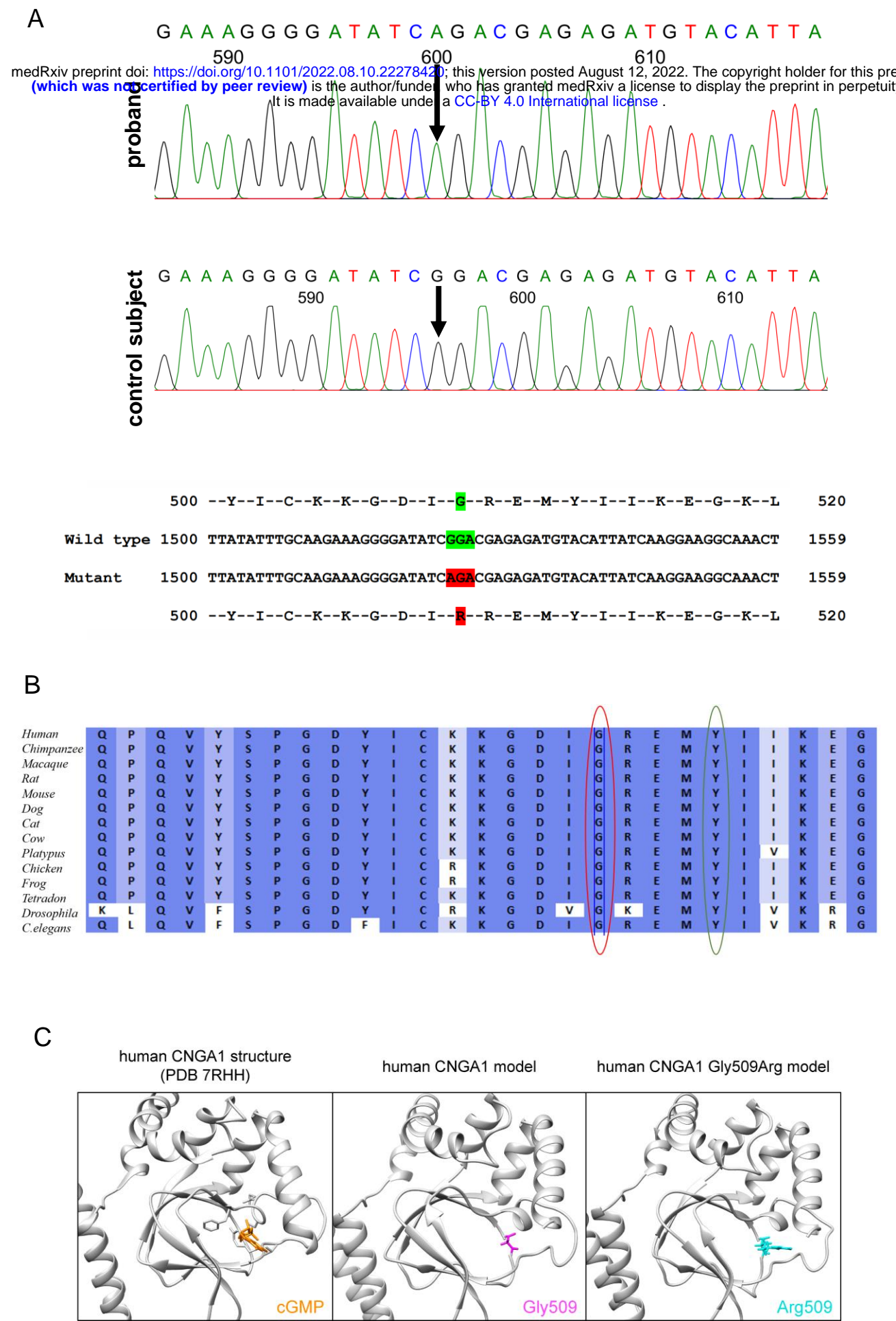
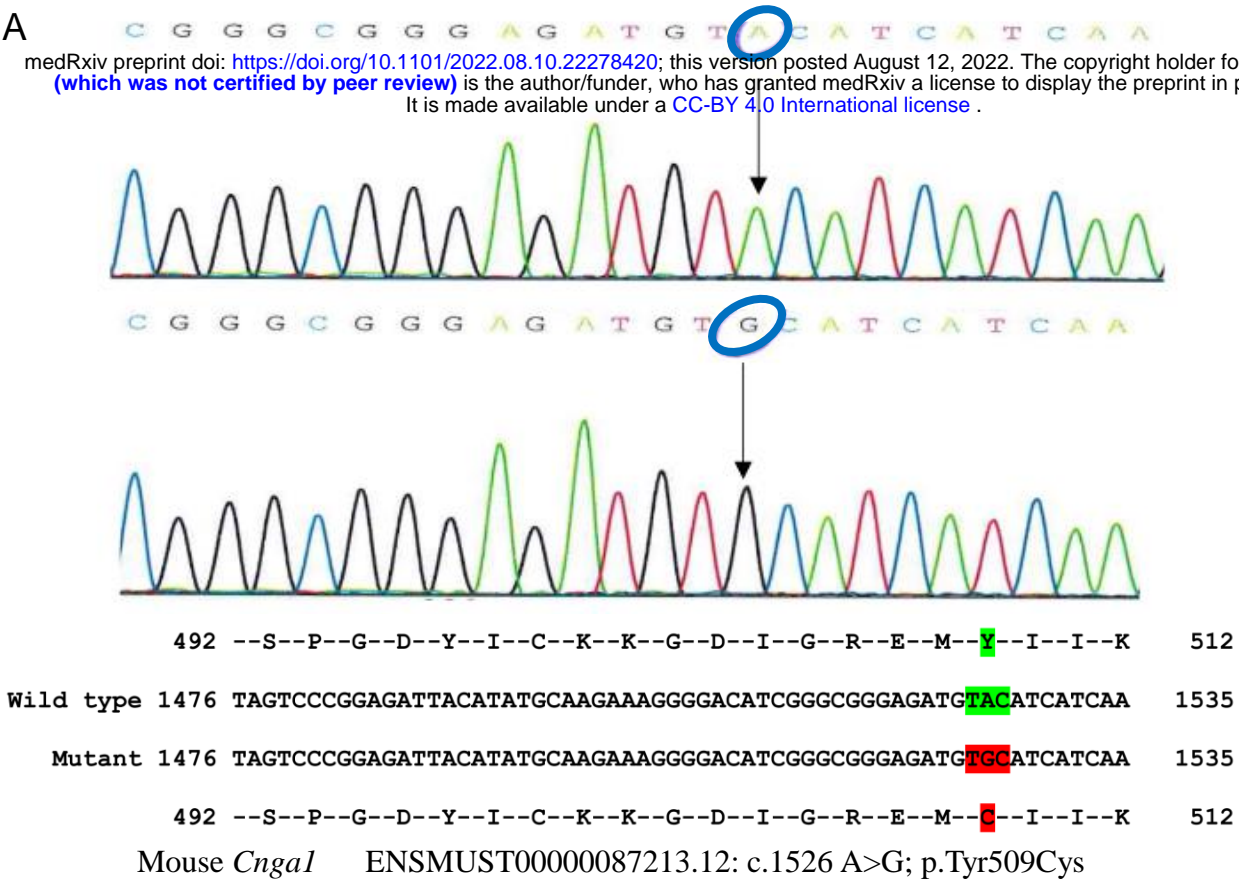


Fig.3

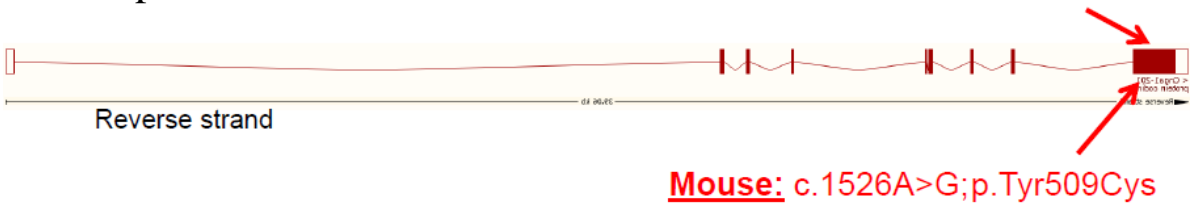
A

medRxiv preprint doi: <https://doi.org/10.1101/2022.08.10.22278420>; this version posted August 12, 2022. The copyright holder for this preprint (which was not certified by peer review) is the author/funder, who has granted medRxiv a license to display the preprint in perpetuity. It is made available under a CC-BY 4.0 International license.



B

Human patient *CNGA1* NM\_001379270.1: c.1525G>A; p.Gly509Arg



C

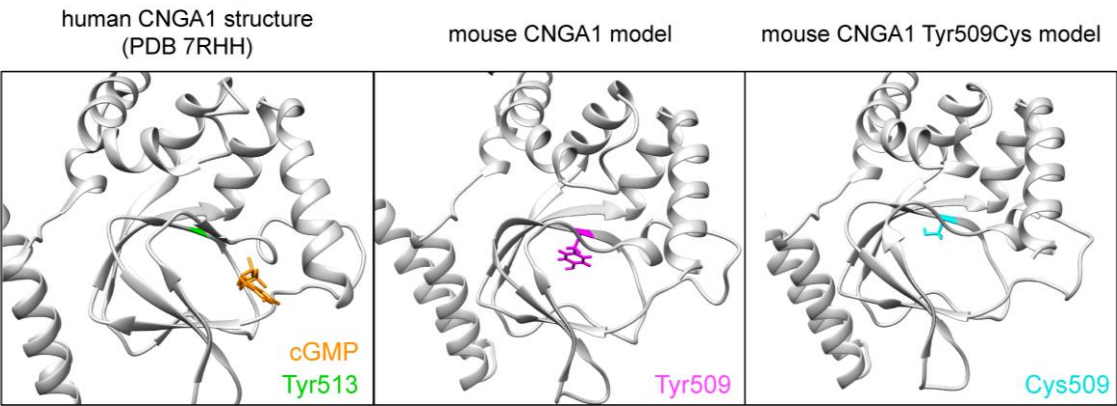
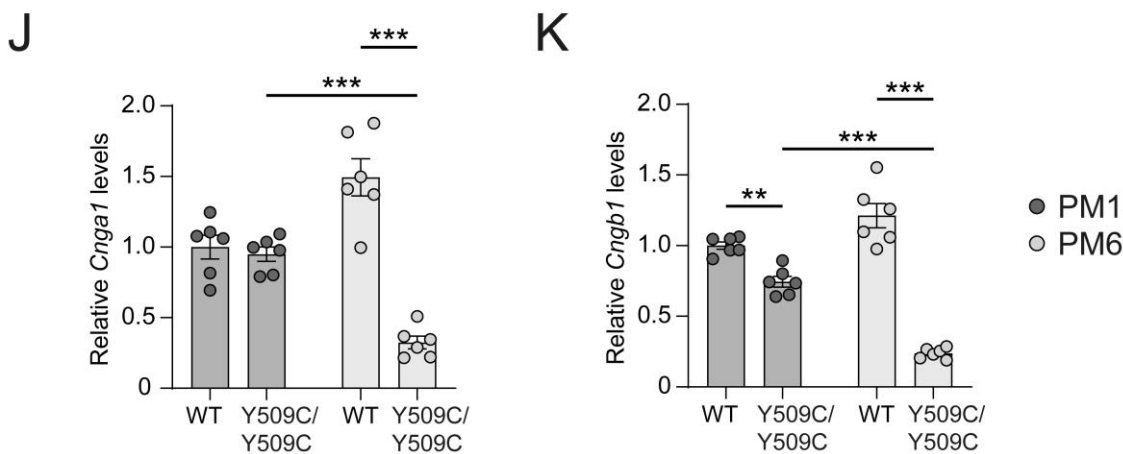
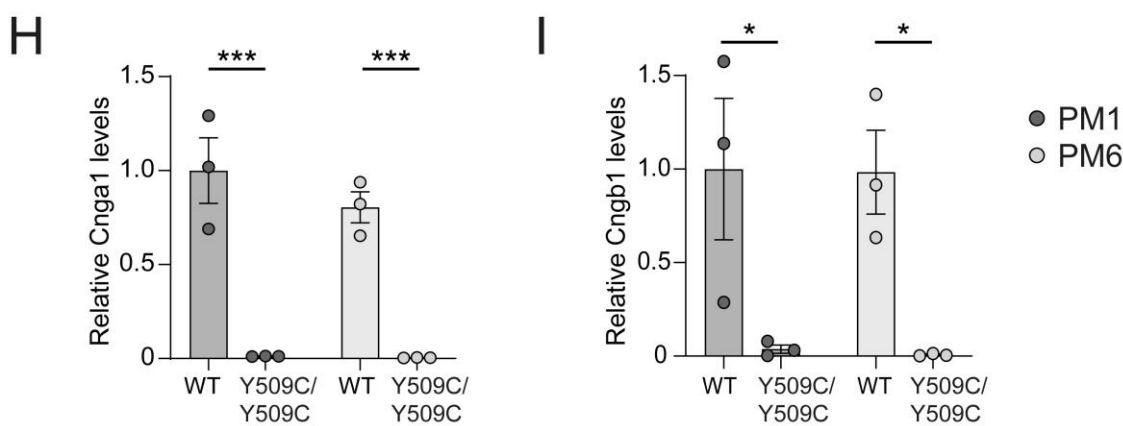
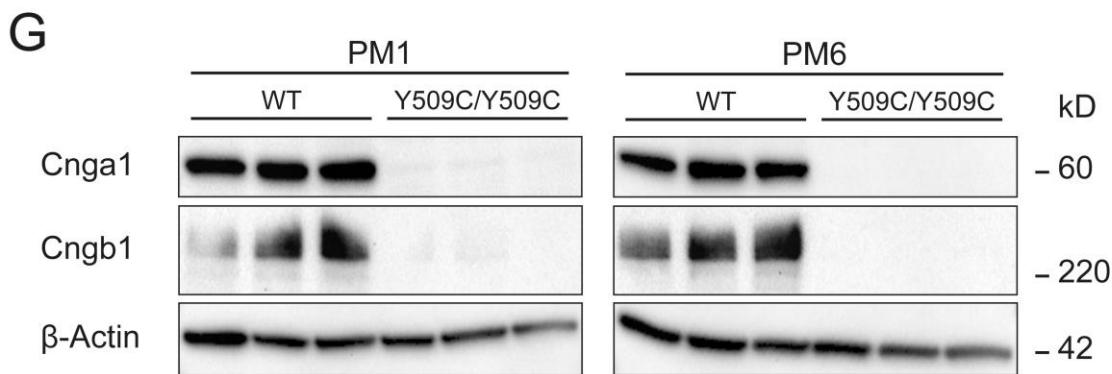
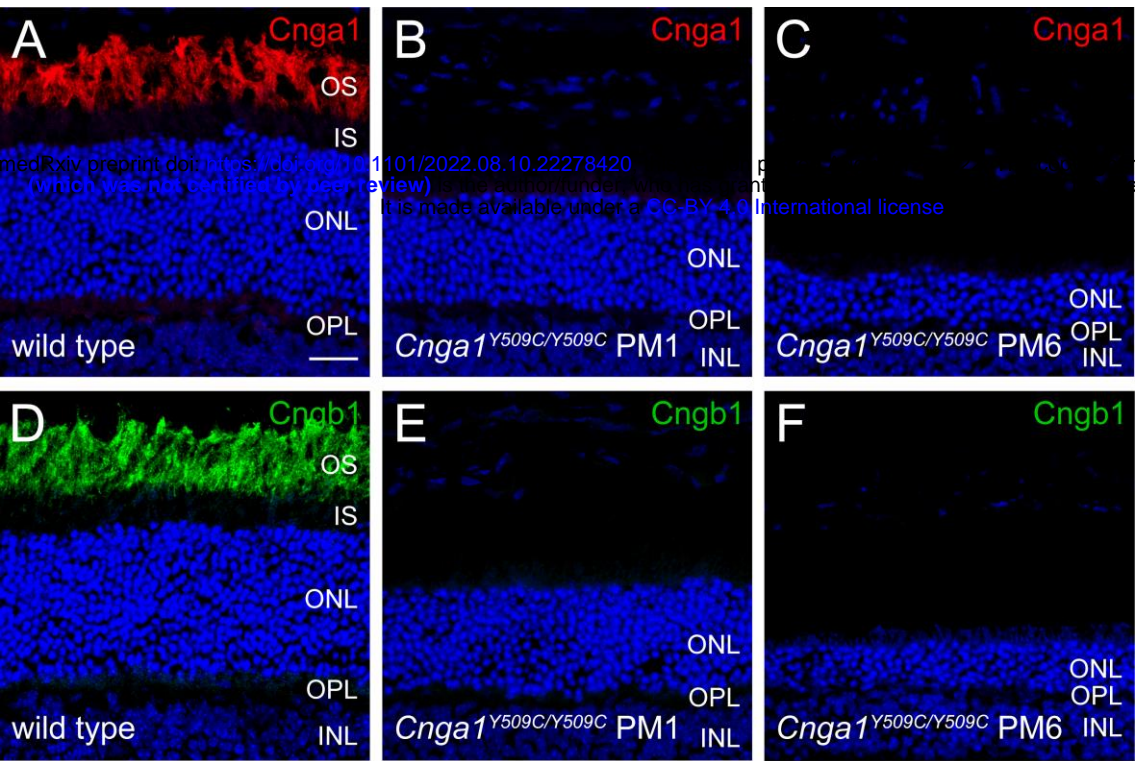


Fig.4



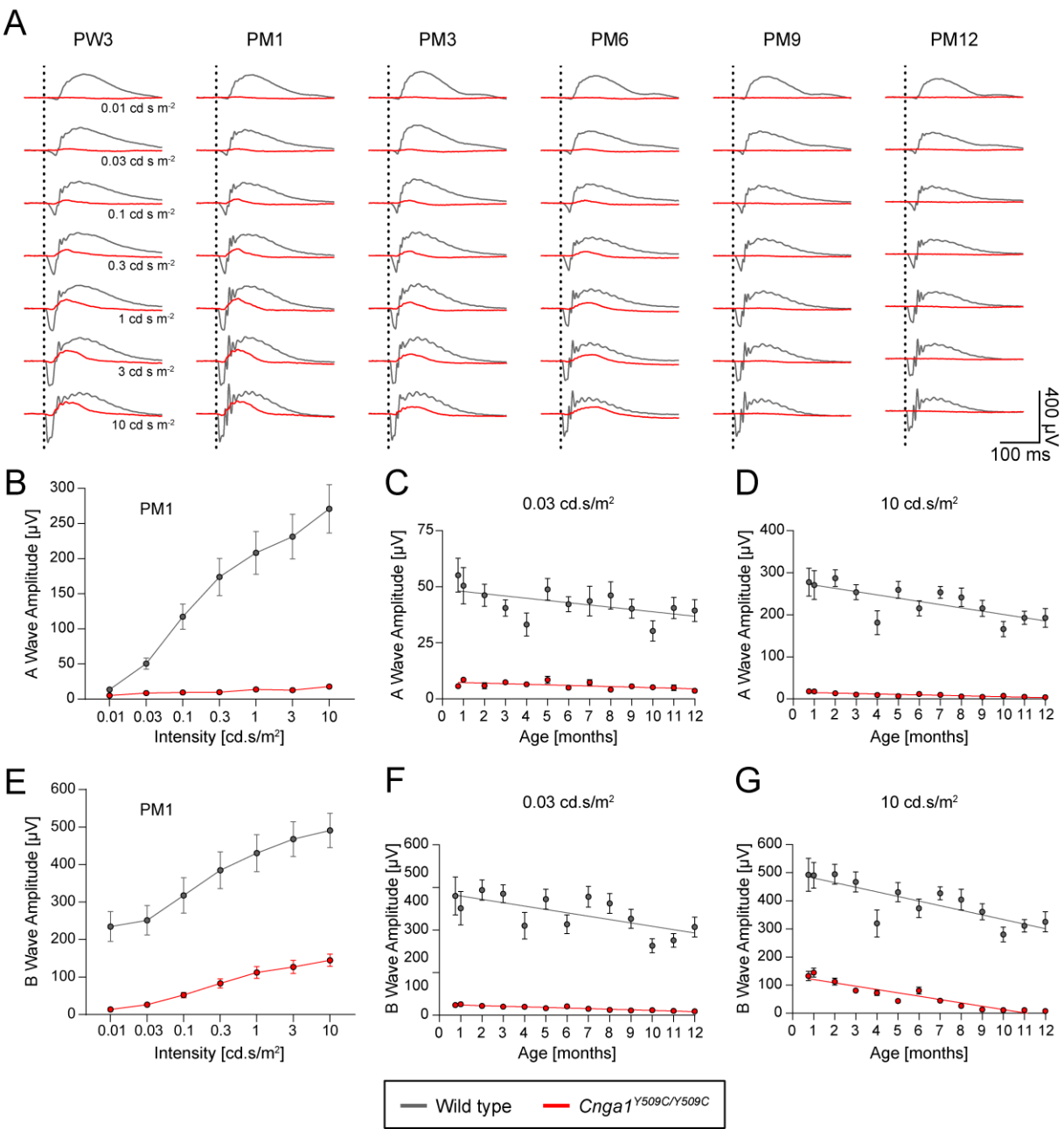


Fig.6

medRxiv preprint doi: <https://doi.org/10.1101/2022.08.10.22278420>; this version posted August 12, 2022. The copyright holder for this preprint (which was not certified by peer review) is the author/funder, who has granted medRxiv a license to display the preprint in perpetuity. It is made available under a CC-BY 4.0 International license.

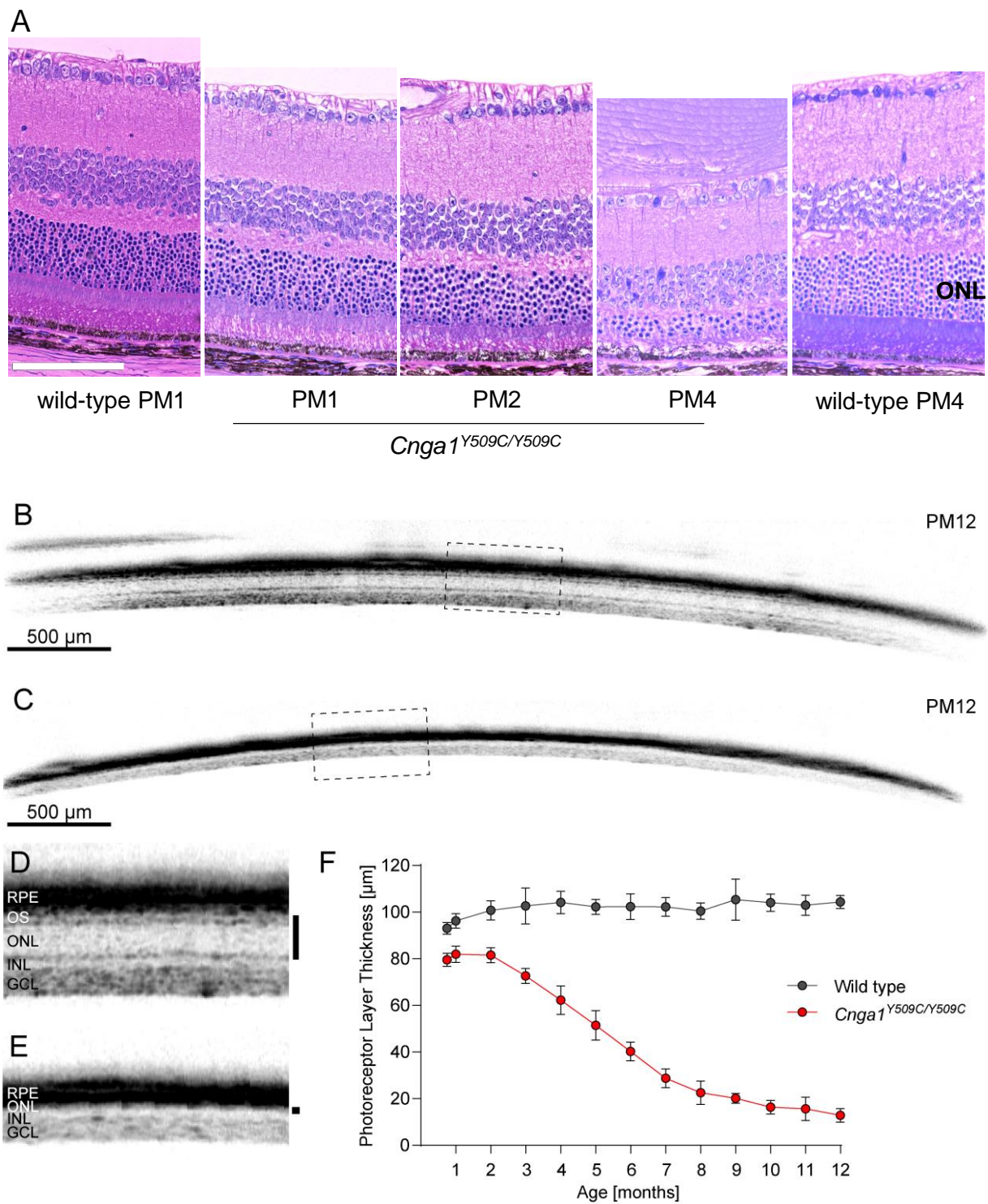


Fig.7

